Journal of Power Sources 684 (2026) 240392

Contents lists available at ScienceDirect

Journal of Power Sources

journal homepage: www.elsevier.com/locate/jpowsour

Local impact of cell degradation on transport and structural properties in the cathode catalyst layer of a polymer electrolyte membrane fuel cell

J. Mitzel [a,*], T. Morawietz [a,b], J.-F. Heger [b], H. Kaess [b], P. Gazdzicki [a]

[a] German Aerospace Center (DLR), Institute of Engineering Thermodynamics, Pfaffenwaldring 38-40, Stuttgart, 70569, Germany
[b] Esslingen University of Applied Sciences, Faculty of Science, Energy and Building Services, Kanalstraße 33, Esslingen, 73728, Germany

HIGHLIGHTS

- Impact of load cycling on degradation of cathode catalyst layer.
- Pt/C catalyst degradation results in 37% active area loss.
- Pore size reduction and local porosity loss results in denser CL structure.
- Increased ionomer concentration leads to 10% increase of O_2 transport resistance.
- Macroscopic ionomer migration as relevant degradation mechanism.

GRAPHICAL ABSTRACT

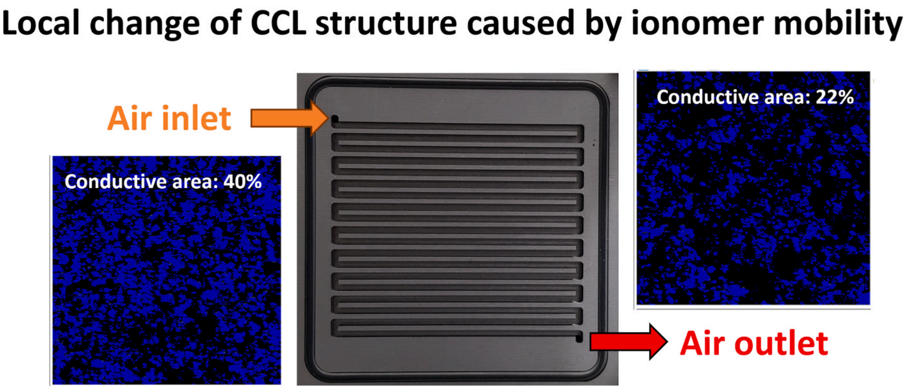

ARTICLE INFO

Keywords:
Cathode structure
Degradation
Ionomer migration
Ionomer mobility
Local effects
Polymer electrolyte membrane fuel cell
Transport properties

ABSTRACT

Fuel cells can be a solution for carbon-free transport, but are affected by high price and limited lifetime. Material level degradation mechanisms are understood but structure changes require more analysis. This study investigates the degradation impact on material, transport and structural properties in the cathode catalyst layer. A 500 h AST using automotive load cycle and conditions (80 °C, 2.5/2.3 bar_{abs}, 50%/30% relative humidity, 1.3/1.5 stoichiometry at anode and cathode) is applied and alterations of these properties are discussed. Whilst the membrane's influence appears to be minor, Pt/C degradation mainly caused the performance decay on the material level (−37% active area). The structural analysis revealed local pore size reduction and a 0.6 μm thick layer at the interface cathode catalyst layer (CCL)/membrane with collapsed porosity. Besides carbon and catalyst degradation, ionomer migration within the catalyst layer during wet/dry cycles cause the pores to fill with ionomer. The local ionomer concentration increased more at humid conditions at air outlet (+59%) and results in decreased proton transport resistance (−38%) and increased oxygen transport resistance (+10%). Consequently, this work reveals that the ionomer macroscopically migrates into the CCL pores during fuel cell operation and this represents an important additional degradation mechanism.

---

* Corresponding author.
E-mail address: Jens.Mitzel@dlr.de (J. Mitzel).

https://doi.org/10.1016/j.jpowsour.2026.240392
Received 19 January 2026; Received in revised form 30 April 2026; Accepted 13 May 2026

1. Introduction

The transition to carbon-free transport and energy sectors requires the use of a carbon-free energy carrier and an efficient energy conversion for different applications. It is widely agreed that hydrogen can be such an energy carrier and fuel cells can convert the chemical energy of hydrogen molecules to electrical energy required to power e.g. electric motors for transport applications. Polymer electrolyte membrane fuel cells (PEMFCs) have proven to be applicable to the dynamic requirements in road transport applications [1]. During the last decades, several barriers have been overcome to enable commercialization [2]. Nevertheless, there are still two main challenges remaining for the PEMFC technology: (i) durability under relevant conditions, such as dynamic conditions in light and heavy-duty vehicles or similar and (ii) targeted costs to be competitive with internal combustion engines (ICE) [3].

One of the main contributions and limitations regarding PEMFC stack cost and lifetime is the catalyst layer (CL) [4]. This CL is composed of carbon supported catalyst and proton conducting ionomer in a porous structure and represents the location where the electrochemical reactions take place. It must provide continuous access of different species to the catalytically active sites, which should be located as much as possible in the so-called triple phase boundary (TPB). Thus, the CL should enable (i) an efficient proton transport via ionomer or water, (ii) a continuous pore network for the transport of reactant gases and product water, and (iii) an electron conducting network [5]. As a result, the CL is heterogeneous and complex and the lifetime targets [6] of 7, 000 h for automotive and even 30,000 h for heavy-duty road applications represent additional challenges regarding material and structure stability under various operating conditions.

The operating conditions at the PEMFC cathode are characterized by high temperature, high humidity and an oxygen-containing atmosphere. In combination with a relatively high cathode potential (typically 0.6 – 0.9 V), degradation processes therefore are more pronounced in the cathode catalyst layer (CCL) than in other MEA components [7]. For this reason, the CCL is the focus of most degradation investigations and is also examined more closely in the presented work.

The associated degradation phenomena are well understood at the material level and include both reversible and irreversible processes [8] [9]. These include damage to the catalytically active material (e.g. Pt) and its support material (e.g. carbon) as well as the ionomer used in the CCL and in the membrane. CL degradation has been widely studied including the importance of spatially heterogenous aging of the CL structure and of the evolution of the CL/membrane interface [10] [11] [12]. Different local operating conditions result in uneven distribution of current density, temperature, radical concentration and water content in the CL and impacts carbon corrosion, Pt sintering and dissolution, ionomer degradation, and CL structure evolution [10]. The ionomer can degrade under high local temperatures, losing the connectivity of proton-conducting pathways and ionomer films can expand and shrink accordingly with the change in its hydration levels. This may lead to the delamination at the three-phase boundary, deactivating the active catalyst sites [13]. Pt/C and ionomer agglomeration, pinholes, and cracks are found in aged CLs [14] [15], which impacts the proton transport or electric network. Furthermore, CL/membrane interfacial delamination can significantly increase the proton transport resistance through this interface [10]. Guilminot et al. [16] reported that delamination and crack formation at the interface is intensified by relative humidity and temperature changes during load cycles. Additionally, the local variation in radical concentration can create localized degradation hotspots resulting in heterogeneous reduction of proton conductivity, formation of voids and cracks, and delamination of layers at interfaces [17].

Regarding structural changes in the CCL, the loss of porosity and the increase of water uptake in the CCL are often referred to a result of carbon corrosion [18] [19] as well as Pt dissolution and redeposition [20], while changes in protonic conductivity are typically referred to ionomer degradation [21] [22] [23]. However, recent publications have shown that the ionomer in the CCL is mobile and can move within the layer. Most publications regarding ionomer mobility are focused on property changes of nanoscale thin-films at catalyst agglomerate level and catalyst/ionomer interactions [15] [24] [25] [26]. But additional publications have shown that ionomer migration is also an important factor for changes of the macroscopic CL structure, like crack formation and propagation, pinhole formation and changes in the porosity. He et al. have demonstrated that the importance of different degradation mechanism can vary upon the operation time under dynamic testing conditions. While catalyst degradation is dominant during the first 100 h, the loss of proton connectivity caused by changes in the ionomer network becomes a main factor for longer fuel cell operation [27]. Wang et al. have shown that fuel cell operation under stationary condition induces also the ionomer/catalyst interface in the CL and state that the mechanism leading to this phenomenon needs further investigation [28]. Additionally, Zhao et al. have performed ex-situ experimental observations of microstructure changes under wet-dry cycling and found considerable growth of the catalyst agglomerates, together with the formation of pinholes and cracks in the CL [14]. The study of Xiao et al. [29] reveals how ionomer degradation contributes to the loss of proton transport networks and pore structures within the CL. Beside crack formation in the CL, it was shown that the volume of primary and secondary pores reduced drastically during 3,000 h fuel cell operation, which was indicated to be a result of a partial CL structure collapse. Consequently, it was stated that ionomer migration and aggregation are the key factors leading to the loss of pore structure. The increase in proton transport resistance is attributed to the loss of a homogeneous network distributions of the ionomer, decreased ionomer thin layers at the catalyst surfaces and chemical degradation of the ionomer.

The study of Yin et al. based on AST measurements targeting CL changes during RH cycling in a climate chamber is of particular interest [30]. It has demonstrated that humidity cycling can induce apparent changes in the CL structure, with ionomer aggregation and migration leading to crack growth and subsequent crack propagation and attributes these changes to ionomer migration.

The work presented here is focused on the identification of degradation phenomena in a technical PEMFC single cell under load cycling conditions including significant gradients in the cathode conditions from air inlet to air outlet regarding oxygen concentration and relative humidity. Local changes in material properties and structural properties are characterized in detail and their impact on electrocatalytic and transport properties are discussed. This includes the consideration of potential ionomer migration depending on the local operating conditions and their influence on the ionomer distribution and the pore structure in the CL as well as on the performance of the analyzed fuel cell. Hence, this work provides new insight into ionomer migration as a mechanism of CL degradation by investigating this phenomenon linked to application relevant local operation conditions.

2. Experimental

2.1. Membrane electrode assembly (MEA)

NC700, a discontinued, ePTFE reinforced membrane with scavenger from Chemours, is used as membrane. The cathode and anode catalyst layers are prepared by a decal method using a knife coater on a PTFE substrate and subsequent hot pressing of the CL to the membrane. Thereby, TEC10E50E (46.2 wt.-% Pt on high surface area carbon) from Tanaka Kikinzoku and D2020CS (20 wt.-% Nafion® dispersion) from Chemours are used as catalyst and ionomer to create catalyst layers with an ionomer to carbon ratio of 0.8. The catalyst loading is set to 0.1 mg_{Pt} cm^{-2} for the anode and to 0.2 mg_{Pt} cm^{-2} for the cathode. On both sides, Sigracet 22BB from SGL Carbon with a thickness of 215 μm, a 5 wt-.% PTFE treatment and a MPL is used as gas diffusion layer (GDL).

2.2. Test cell and test equipment

The test cell consists of graphite composite plates equipped with a single serpentine flow field (rib width 0.8 mm, channel width 1.4 mm, channel depth 1.4 mm) and an active area of 22.5 cm^2 (4.5 × 5.0 cm^2). Thus, the used cell represents a technical single cell and the single serpentine flow field results in a significant gradient in the cathode conditions from air inlet to air outlet. While the cell temperature is kept constant, the oxygen concentration decreases due to oxygen consumption and the relative humidity increases due to produced water along the flow channel. The flow plates are integrated in a liquid cooled quickCONNECT qCf FC25 cell and cell fixture from balticFuelCells GmbH. The compression force on the MEA is pneumatically controlled to achieve 1 MPa. Hydrogen (5.0 quality by Linde AG) and air (dried, filtered, and compressed ambient air) are supplied in counter flow configuration. Additionally, nitrogen (5.0 quality by Linde AG) is used for electrochemical characterization.

The in-house developed test stand controlled by programmable logic controllers allows automatic control of the test conditions, such as the pressure, temperature, gas flow rates and humidity. The commercial electronic load ZS506-4NV-SV5 from Höcherl & Hackl GmbH was used to control cell current density. The gasses are humidified by bubblers according to the respective dew point temperature. The reactant pressures are measured and controlled at the cell outlets.

2.3. Degradation test protocol and test conditions

The durability test is performed according to the EU Harmonized Test Protocols for PEMFC MEA testing in single cell configuration for automotive applications [31]. The related reference operating conditions are summarized in Table 1.

The durability is evaluated by imposing the Fuel Cell Dynamic Load Cycle (FC-DLC) as shown in Fig. 1a for 500 h including start-up and shutdown cycles. This test cycle consists in 35 load steps defined as percentage of the maximum current density [20], which is determined to 1.05 A cm^{-2} from the current response at 0.65 V in the BoT polarization curve (Fig. 2a and Table S1). The degradation rates during the test are determined at 3 different load levels (0.05, 0.44, and 1.05 A cm^{-2}), indicated in Fig. 1a. Each FC-DLC is about 20 min (1181 s) and the test is structured in test blocks interrupted by short stops after 6 cycles and long stops after 4x6 cycles to simulate a realistic drive cycle (Fig. 1b).

The short stops last 10 min without cell cool down and include load disconnection, pressure reduction to ambient pressure, stopped air flow (hydrogen flow maintained to assure cell voltage decrease). The long stops last 4 h with cell cool down to 20 °C. Again, the load is disconnected, the pressure is reduced, and the air flow is stopped. Additionally, the hydrogen flow is stopped after 10 min, but the cell voltage still remains below 0.1 V. An example for short and long stop is shown in Fig. 1c.

It should be mentioned that nitrogen purges are not used in this degradation test protocol to enable degradation behavior close to automotive application. Nevertheless, it is well known that the cell degradation is accelerated by this test protocol due to fast and frequent load, pressure and temperature variations [32] as well as present hydrogen/air fronts in the cell during start-up [33].

Table 1
Test conditions applied for durability test, polarization curve and EIS measurements.

	Conditions
Cell temperature/°C	80
Gas composition	H_2/Air
Pressure at anode and cathode outlet/bar$_{abs}$	2.5/2.3
Gas inlet temperature at anode and cathode/°C	85/85
Relative humidity at anode and cathode inlet/%	50/30
H_2 and O_2 stoichiometry/-	1.3/1.5
Min. gas flow according to current density/A cm^{-2}	0.4

2.4. Electrochemical characterization

The electrochemical properties of the examined MEA are determined at begin-of-test (BoT) and end-of-test (EoT) including measurements for performance (polarization curve), electrochemical impedance spectroscopy (EIS), high frequency resistance (HFR), and hydrogen cross-over as well as for effective proton transport resistance ($R_{eff,H+}$) and roughness factor of the catalyst (RF) in the CCL. In addition to the used test stand, electrochemical analysis was realized using a combination of IM6 and PP241 potentiostats from ZAHNER-elektrik GmbH & Co. KG. Data acquisition and analysis were carried out using the Thales XT 5.8.2 software.

Polarization curves and EIS are measured applying the same conditions as used for the degradation test (Table 1). The polarization curve protocol is following the EU-harmonized protocol [17] using galvanostatic steps with dwell times of 60 s below 0.1 A cm^{-2} and 120 s above 0.1 A cm^{-2}. Resulting voltage values are extracted as the average value during the last 30 s. EIS measurements are also realized galvanostatically applying various DC load levels and AC amplitudes (Table 2) between 50 kHz and 100 mHz (varied from high to low frequency). The presented parameters of HFR, oxygen reduction reaction (ORR) charge transfer resistance and O_2 mass transport resistance are extracted from the EIS data using Thales XT 5.8.2 and the equivalent circuits presented in Fig. S1.

All EIS measurements (in H_2/air and H_2/N_2) are realized after at least 5 min stabilization. Measurements were realized using 10 steps per decade and 20 measure periods above 66 Hz as well as 5 steps per decade and 4 measure periods at lower frequencies. Linearity and stability are checked according to Kramers-Kronig relations. EIS results are presented in the main document via Nyquist plot. Related Bode plots are included in the supplementary information to present frequency-dependent behavior.

The hydrogen cross-over is estimated from a chronoamperometric measurement of the oxidation current caused by permeating hydrogen from anode to cathode using different conditions. Thereby, the cell is fed by 113 mL min^{-1} (5 mL min^{-1} cm^{-2}) hydrogen to the anode and 45 mL min^{-1} (2 mL min^{-1} cm^{-2}) nitrogen to the cathode while polarizing the cathode to 0.4 V for 5 min. The cross-over values are extracted by the average value during the last 2 min.

$R_{eff,H+}$ and HFR are measured using the same gas flows as used for hydrogen cross-over. The measurements are realized at 80 °C, 1500 $mbar_{abs}$ on anode and cathode side, and variable relative humidity (RH) of 50%, 80%, and 100%. $R_{eff,H+}$ is extracted from potentiostatic EIS measurements at 0.4 V with an amplitude of 5 mV between 25 kHz and 10 Hz (varied from high to low frequency) using the transmission line model suggested by Pickup et al. [34] [35] (see Fig. S2). It can be obtained from the magnitude of a Warburg-like region projected onto the x-axis (x_{war}) corrected by HFR in a Nyquist plot using Eq. (1).

$$R_{eff,H+} = 3 * (x_{war} - HFR) \qquad \text{Eq. 1}$$

The RF of the platinum catalyst in the CCL is determined by cyclic voltammetry (CV). CVs are measured using the same gas flows as used for hydrogen cross-over at 30 °C, 1000 $mbar_{abs}$, 100% RH. The scan rate was varied to 20, 50, 100, and 200 mV s^{-1} and the RF was calculated using Eq. (2).

$$RF = q_{H-ads} \ / \ (\Gamma * A_{geo}) \qquad \text{Eq. 2}$$

$q_{H\text{-}ads}$ represents the charge determined by integration of the hydrogen adsorption peaks (see Fig. S3) and A_{geo} is the geometric active area of the examined electrode (22.5 cm^2). The charge $\Gamma = 210\ \mu C\ cm_{Pt}^{-2}$ is required for the electrochemical adsorption of one monolayer hydrogen on a polycrystalline platinum surface, also applicable for carbon supported platinum nanoparticles [36] [37].

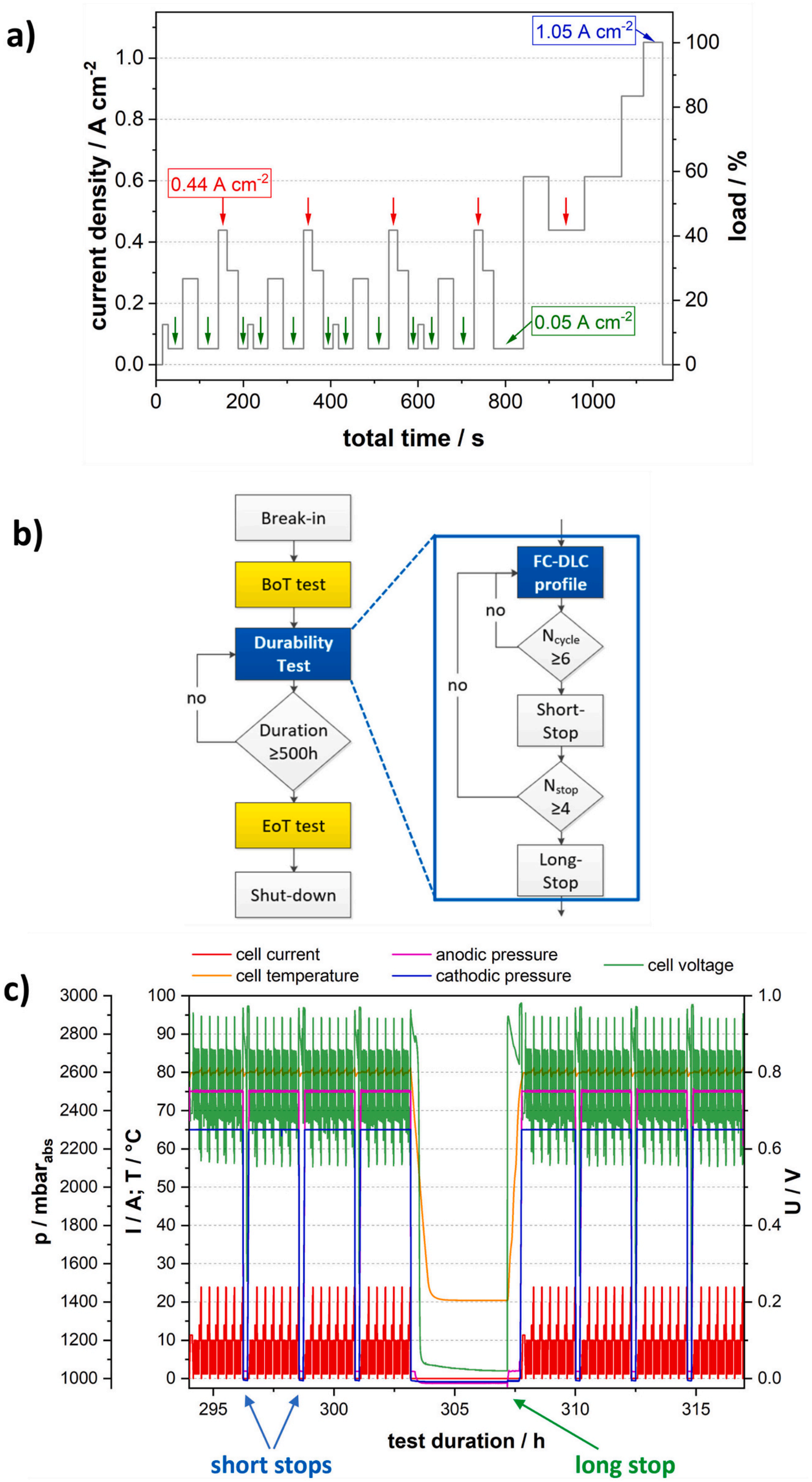

Fig. 1. (a) Load profile of one single FC-DLC sequence including 3 marked load levels used for the calculation of the degradation rates in Fig. 2c. (b) Flow chart of applied 500 h degradation test. (c) Example for short and long stop in the applied test profile.

Additionally, the double layer capacity C_{dl} was extracted from the same CVs [38] [39]. C_{dl} was determined according to Eq. (3).

$$C_{dl} = I_{dl} / v \qquad \text{Eq. 3}$$

I_{dl} represents the current in the double layer region at 0.45 V (see Fig. S3) corrected by the hydrogen crossover current (average between up-scan and down-scan) and v is the voltage scan rate of the CV measurement.

2.5. *Scanning Electron Microscopy*

Scanning Electron Microscopy (SEM) measurements were performed using a Jeol 7200F FE electron microscope with E-T detector. Prior to

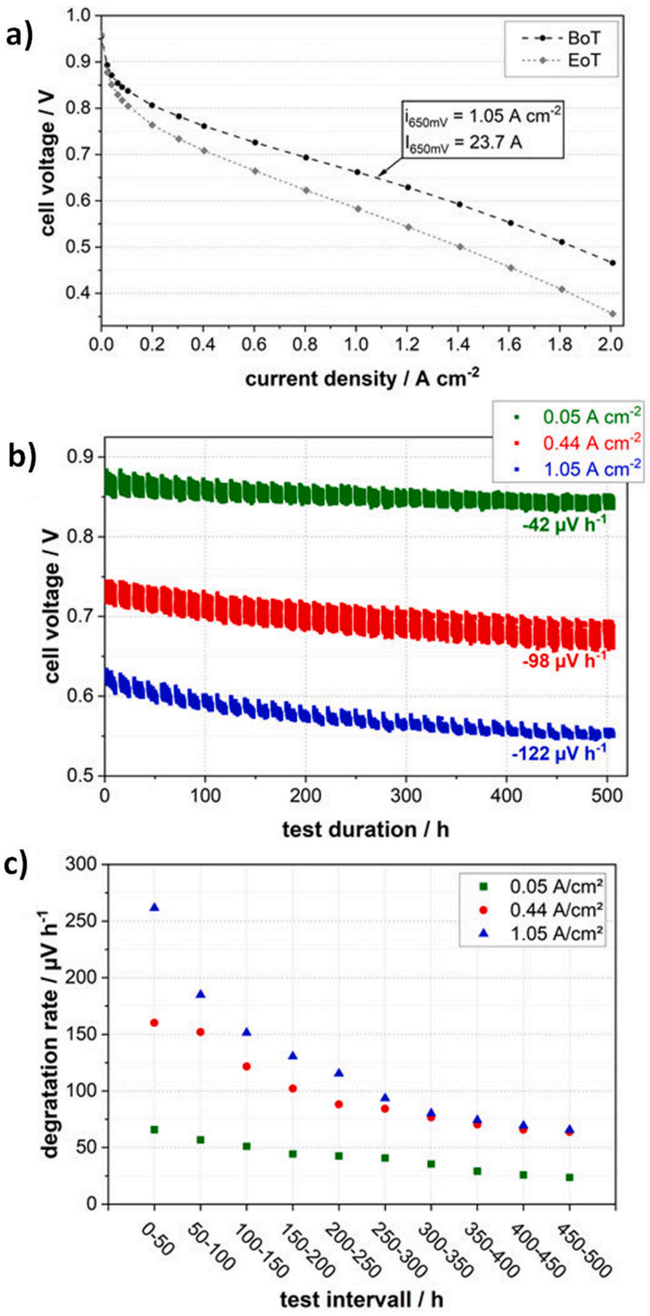

Fig. 2. Degradation behavior of PEMFC MEA during the 500 h load cycling test. (a) Polarization curves Begin-of-Test (BoT) and End-of-Test (EoT) in automotive conditions (Table 1) after recovery of reversible voltage losses. (b) Voltage values and degradation rates at different load levels during FC-DLC durability test. (c) Time-dependent degradation rates during each 50 h interval calculated from (b).

Table 2
DC load and AC amplitude parameters applied for EIS measurements.

Current density/A cm^{-2}	DC load/A	AC amplitude/A
0.025	0.563	0.03
0.2	4.5	0.2
0.5	11.3	0.5
1.0	22.5	1.0
1.5	33.8	1.0

the measurements, the samples were cut with Jeol ionmilling device at 6 kV through the whole MEA while the stage was swinging. The samples were in addition sandwiched between two silicon wafers to increase the stability while cutting. The measurements were performed with 5 kV and a WD of 10 mm. In addition, FIB-SEM was performed using Zeiss Crossbeam 350 microscope with Gallium FIB. The area of examination was covered with platinum using gas injection system and tracking marks for drift compensation were added and then covered with carbon also using the gas injection system. With 3 nA a coarse trench was cut into the electrodes, then the fine trench was prepared with 700 pA. The milling beam for tomography was chosen to be at 30 kV/300 pA with a slice thickness of 5 nm, same as the pixel size. Imagin of each slice was performed using SE detector at a WD of ~5.1 mm (coincidence point of FIB and electron beam) with acceleration voltage of 2 kV. Drift compensation was done every 3 slices. Evaluation of the volumes was performed with GeoDict 2026 using the included AI algorithm in the module ImportGeo for import and segmentation. Porodict was used to evaluate the pore space.

2.6. *Atomic Force Microscopy*

Atomic Force Microscopy (AFM) measurements were performed using Multimode 8 and Icon XR AFMs on the same samples used for SEM measurements. NCH-Pt (Nanosensors) tips with a nominal spring constant of 42 N/m were used to measure the cross-sections and surfaces in PF-TUNA mode, which measures the mechanical properties in addition to the electronic conductivity. For measuring the surface, it was connected with an additional carbon tape to ensure conductivity of the top layer to the sample puck. In addition, for high resolution mapping of the porosity and detecting ionomer at the nanoscale supersharp tips with 5 N/m were used (SHR150, Budgetsensors).

An algorithm developed specifically for this purpose processes AFM height images to extract surface porosity. It subtracts a Gaussian-smoothed background from each image to isolate surface depressions, identifies pores using a threshold-based method, and calculates porosity as the fraction of pore pixels relative to the total image area.

3. Results and discussion

3.1. *Performance decay during fuel cell operation*

Fig. 2 shows the degradation behavior of the MEA during the applied 500 h load cycling degradation test. The performance decay is demonstrated by the comparison of the BoT and EoT polarization curves in Fig. 2a. Obviously, the MEA degraded significantly due to the AST approach of the applied test. A voltage loss up to 110 mV at 2.0 A cm^{-2} was detected. Both polarization curves are measured after cell shutdown and cool-down as well as electrochemical characterization. Therefore, it can be assumed that reversible voltage losses from the 500 h degradation test are fully recovered and the demonstrated voltage decays are only caused by irreversible degradation processes [8].

Fig. 2b represents the voltage decay during the 500 h FC-DLC test including both, reversible and irreversible degradation processes. Voltage values at 3 different load levels were extracted from the test data, without considering the 3 s before and after each load change to exclude capacitive effects. The relatively high total degradation rates in the range −42 up to −122 μV h^{-1} also demonstrate the AST character of the applied test. The resulting voltage decay is non-linear and therefore time-dependent degradation rates during each 50 h interval are presented in Fig. 2c.

A closer look on the polarization curves in Fig. 2a reveals a voltage decay already in the ORR charge transfer dominated regime below 0.1 A cm^{-2}, which suggests that the catalyst is impacted by the applied test. The voltage decay at 0.05 A cm^{-2} is included in Fig. 2b and the total degradation rate during the 500 h test is about −42 μV h^{-1}, resulting in a voltage loss of about 21 mV during 500 h. This is in good agreement with the difference between BoT and EoT performance in Fig. 2a. Due to the mentioned recovery of the reversible voltage losses before polarization curve measurements, the performance loss at low current density seems to be caused by irreversible degradation phenomena. The corresponding time-dependent degradation rates extracted from the durability test data (Fig. 2c) show an almost linear decrease from 66 to 24 μV h^{-1}.

In contrast, the voltage decays at 0.44 and 1.05 A cm^{-2} in Fig. 2b are clearly not linear and higher compared to 0.05 A cm^{-2}. In general, the voltage decay and thus the performance loss are more pronounced with increasing current density. At 0.44 A cm^{-2}, -98 μV h^{-1} results in a voltage loss of about 49 mV during 500 h, which is again in good agreement with the difference between BoT and EoT performance (Fig. 2a) and thus should be caused by irreversible degradation phenomena. Fig. 2c demonstrates that the time-dependent degradation rates at this load level decrease non-linearly from 160 to 64 μV h^{-1}.

At 1.05 A cm^{-2}, which is defined as maximum current density during the FC-DLC protocol, the total degradation rate corresponds to −122 μV h^{-1} resulting in a voltage loss of about 61 mV during 500 h, which seems to be partially reversible. This reversible voltage recovery is typically based on the removal of oxides and impurities from the catalyst surface, varied water management within the membrane and electrodes, and the associated structural changes in the membrane and the catalyst layer [8]. The voltage decay and the trend of the degradation rate over time show clearly non-linear behavior. Furthermore, the degradation rates decrease significantly from 262 to 66 μV h^{-1}. It is well known that the performance in this load range is also limited by the oxygen mass transport in the cathode [40]. It can be assumed that the change in the corresponding transport properties is also not linear with time and is more pronounced at the beginning of the test. These transport properties are typically dominated by the CL structure. Thus, changes in this structure are of high importance for the understanding of the appearing degradation mechanisms and are an essential part of the presented work. The impact of the degradation test on the different materials and on the CL structure will be discussed in the following.

3.2. *Impact on membrane properties*

Fig. 3a and b show cross-section images of a pristine CCM samples (BoT without compression in the used single cell) and after the 500 h degradation test (EoT including compression in the test cell) recorded by SEM, respectively. The latter shows 50-100 nm platinum particles formed in the membrane near the cathode/membrane interface during the test (Fig. 3c).

Thereby, significantly more and larger platinum particles are formed at the air outlet (hydrogen inlet) which is in agreement with previous studies [41]. The existence of these particles, also known in the literature as platinum band [42] [43], enables the chemical recombination of hydrogen and oxygen inside the membrane. This reduces the hydrogen crossover current (Fig. 3d), which is particularly evident at an increased pressure of 2300/2500 $mbar_{abs}$ with a reduction of about 0.7 mA cm^{-2} (7.5%) between BoT and EoT. Furthermore, the formation of these particles near the cathode/membrane interface, especially close to the air outlet, indicates that parts of the catalyst in the CCL undergoes Pt dissolution and migration into the membrane which is consistent with the RF loss discussed later.

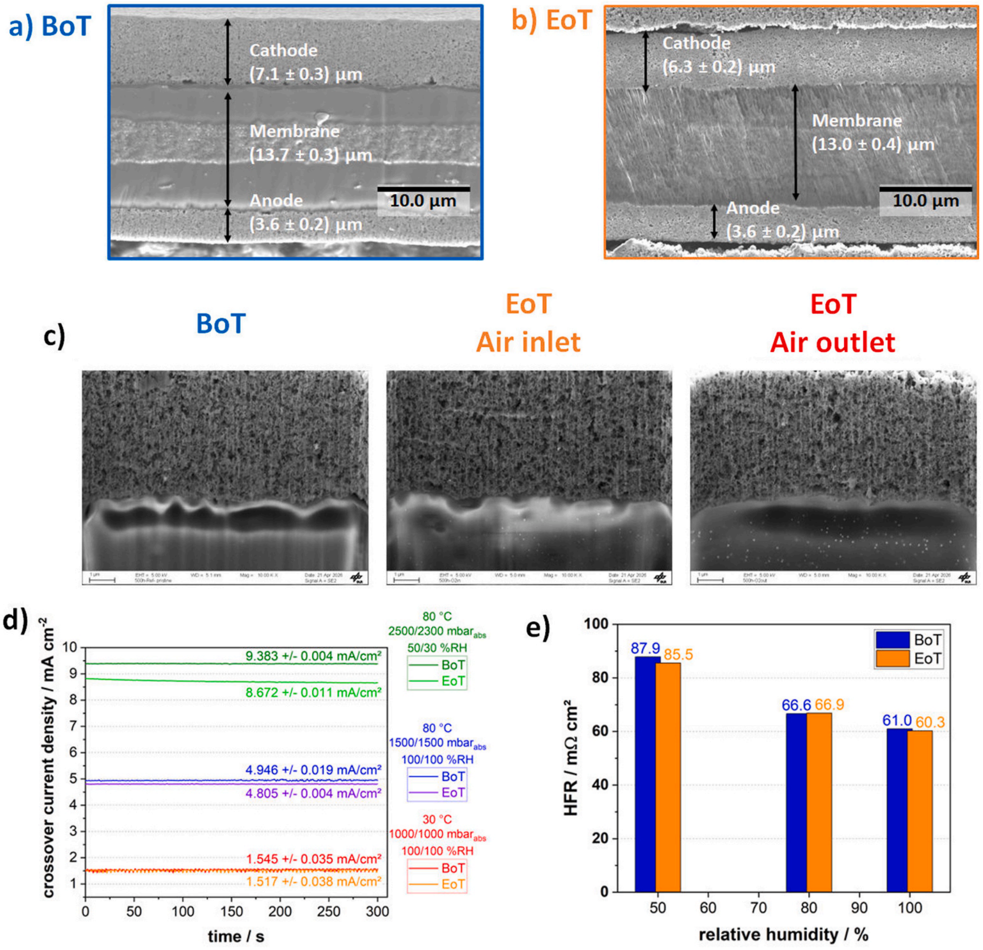

Fig. 3. Impact of 500 h degradation test on catalyst coated membrane (CCM) and membrane properties: (a) BoT and (b) EoT cross-section SEM images of the CCM. (c) Visualization of Pt band via SEM at cathode/membrane interface. (d) Hydrogen crossover current density under different conditions. (e) HFR measured in H_2/N_2 atmosphere at 80 °C and 1500 $mbar_{abs}$ using variable RH.

The change of CL and membrane thicknesses observed in Fig. 3a and b need to be taken with care, since the pristine cell was not compressed. Nevertheless, a thinning of the membrane by 5% and a thinning of the cathode thickness by 11% was determined, while the anode thickness is not affected (3.6 μm). Hence, it is not sufficient to state that the change in the CCL thickness is caused by cell compression alone. On the other hand, the reduced membrane thickness should lead to a reduction in the HFR during fuel cell operation. However, no significant reduction was detected in the corresponding measurements as shown in Fig. 3e. Nevertheless, it is noted that HFR is not only a property of membrane thickness; it represents the sum of all ohmic resistances in the cell. In addition to the membrane thinning, HFR can be impacted by: (i) water content in the membrane [44], (ii) chemical membrane degradation resulting in loss of sulfonic acid groups of the ionomer [45], and (iii) increase of the contact resistances between the cell components [46].

Generally, it can be concluded that the increase of voltage loss with increasing current density in the polarization curves shown in Fig. 2a cannot only be caused by increased ohmic resistance. Hence, membrane degradation seems not to be the main reason for the performance loss. Additional analysis such as the determination of the fluorine emission rate could allow further conclusions about the membrane behavior. However, this was not the focus of the presented study. On the other hand, the loss of CCL thickness and the formation of a Pt band close to the cathode/membrane interface suggests that degradation effects of the catalyst and/or of the CCL structure occurred. This will be discussed in the following.

3.3. Impact on catalyst properties

The decreased performance at low current density, i.e. in the ORR charge-transfer dominated regime, as well as the formation of the platinum band in the membrane suggests that the catalyst degraded during the 500 h test. CVs at different scan rates of 20, 50, 100, and 200 mV s^{-1} (Fig. 4a) are used for further investigation. The resulting RFs in the CCL (Fig. 4b) at different scan rates are very similar and thus the RF values can be considered as independent from the used scan rate. This demonstrates that the integrated peaks (Fig. S3) are caused by the complete electrochemical adsorption of a hydrogen monolayer on the platinum catalyst and that there is no limitation due to mass transport or reaction kinetics. In addition, the integration result is thus not superimposed by faradaic reactions such as hydrogen evolution and the determined RFs can be considered reliable [47]. The averaged RF values are reduced from (134.1 ± 2.4) to (84.6 ± 1.3) cm^2_{Pt} cm^{-2}_{geo} by about 37% during the 500 h test. This loss in active catalyst surface can be caused by growth of the catalyst particles in the CCL, by Pt dissolution and redeposition in the membrane [38], and by changes in the CCL structure with impact on accessibility of the catalytic sides to the oxygen and/or the protons [48].

EIS measurements at very low current density of 0.025 A cm^{-2} (Fig. 4c and Table S2) confirm the significant loss of catalyst activity during the 500 h test by an increase of about 24% in the ORR charge-transfer resistance from 1307 to 1622 mΩ cm^2.

The impact of the degradation test on the double layer capacity C_{dl} of the CCL is shown in Fig. 4d. Again, the C_{dl} is independent of the scan rate and not superimposed by faradaic reactions. The difference between the averaged C_{dl} at BoT and EoT is negligible and changes from (36.0 ± 1.4) to (36.3 ± 1.3) mF cm^{-2}_{geo}. According to Iden and Ohma [49], the determined C_{dl} is the result of four interfaces within the CCL, which are Pt/ionomer, Pt/water, carbon/ionomer, and carbon/water. Thus, it is not possible to evaluate, if one of these interfaces changed, but it can be stated that the summation of the C_{dl} of these four interfaces is not affected by the durability test.

It can be summarized that the electrocatalyst in the CCL is strongly degrading during the 500 h test. The RF reduction by 37% and the resulting 24% increase of the ORR charge-transfer resistance causes the occurring performance loss, especially at low and medium current density. Due to the reduced RF, the C_{dl} caused by the Pt/ionomer and Pt/water interfaces can be expected to decrease. However, since the total

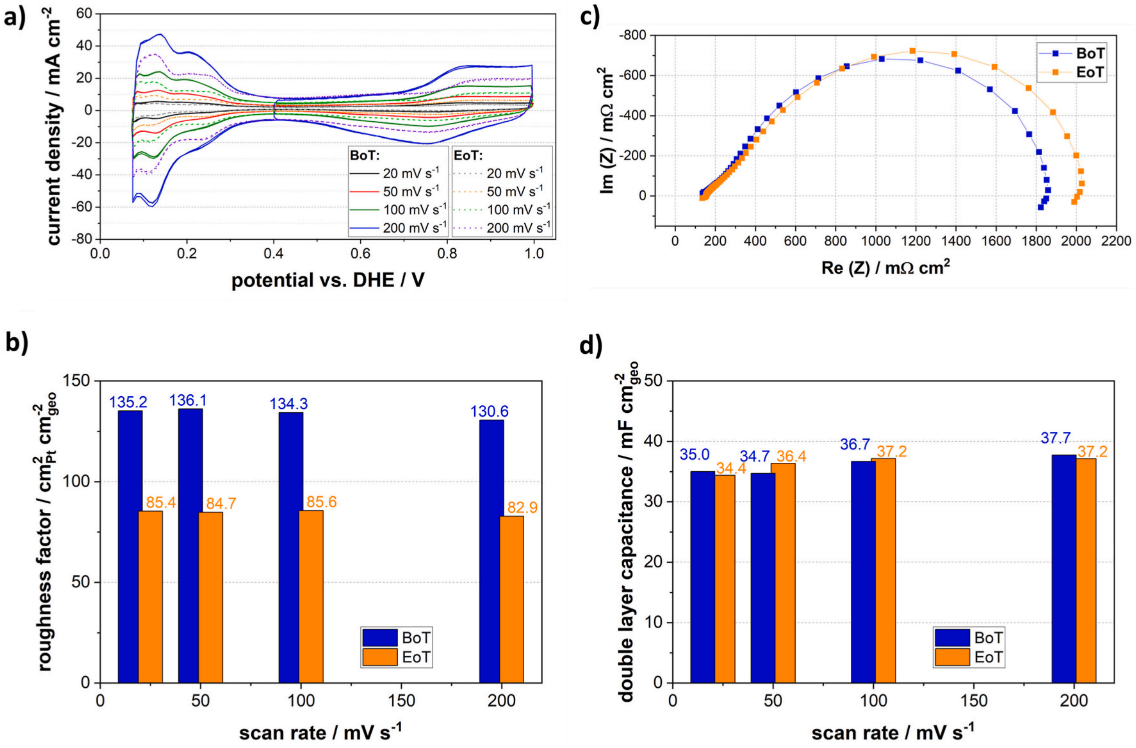

Fig. 4. Impact of 500 h degradation test on catalyst properties: (a) BoT and EoT cyclic voltammograms at 30 °C, 1000 $mbar_{abs}$, 100% RH and different scan rates and (b) resulting roughness factors as well as (d) resulting double layer capacitance. (c) BoT and EoT EIS measurements at 0.025 A cm^{-2} using automotive test conditions presented via Nyquist plots (Bode plots are presented in Fig. S4).

C_{dl} remains unchanged, the C_{dl} caused by the carbon/ionomer and carbon/water interfaces presumably increases. This could have two reasons. Firstly, the carbon support in the CCL could be corroded, which reduces its hydrophobicity and increases the contribution from the carbon/water interface [50]. Secondly, the structure and the ionomer distribution in the CCL could have changed, which influences the contribution through the carbon/ionomer interface [51].

3.4. *Impact on catalyst layer structure*

There were already hints during the evaluation of the impact of the 500 h degradation test on the performance and on the catalyst properties that the CCL structure might be impacted as well. In order to confirm this hypothesis, investigations were first carried out on CCM cross-sections (Fig. 5). This revealed clear differences between the BoT and EoT samples, although these were mainly limited to the CCL structure near the cathode/membrane interface and were more pronounced close to the air outlet. The cross-section analysis at air inlet is based on SEM (Fig. 5a) as well as AFM height profiles (Fig. 5b). While the CCL structure of the BoT sample is quite homogeneous, the EoT sample shows a denser layer close to the membrane interface. This layer is visualized in the cross-section analysis using SEM and AFM by the red, dashed line. To enable a more quantitative analysis, Fig. 5c shows line scan sections in x and y direction following the lines indicated in Fig. 5b. The position of the cathode membrane interface is marked in the resulting y-sections by the black arrows. It is obvious that the pores are homogeneously distributed in the BoT sample and extend to the membrane. In contrast, the EoT sample shows no clear porosity of the CCL at distances up to 0.6 μm from the membrane, representing the mentioned denser layer. Additionally, the x-sections of Fig. 5c enable the determination of the pore size distribution in the CCL close to the membrane. Height differences of about 50 nm were detected in the BoT sample. In contrast, the height differences at EoT correspond to only 30 nm. Thus, the 500 h test resulted in a local reduction of the pore size by ~40%. Related to the entire CCL thickness (6.3 μm), the thickness of this local degraded areas (0.6 μm) corresponds to about 10% of the CCL thickness.

Fig. 5d shows a detailed investigation by AFM deformation and height analysis of this phenomenon at the membrane/CCL interface. The distribution of ionomer and catalyst in the BoT CCL is very homogeneous and shows no gradient towards the membrane. In contrast, the ionomer concentration in the EoT CCL is significantly higher near the membrane, and the formation of the dense layer with low porosity close to the membrane can be confirmed.

In order to assess the changes in the pore structure during the 500 h degradation test more in detail, FIB-SEM analyses of the CCL structure in the immediate vicinity of the membrane were carried out (Fig. 6). The reconstructed 3D structures in Fig. 6a already demonstrate that the porosity of the CCL decreases significantly in this region and that this decrease is more pronounced at the air outlet. The pore size distribution determined from these measurements and shown in Fig. 6b also indicates that the average pore diameter decreases at the air outlet and that only very small pores remain available for gas transport. This further confirms the formation of a very compact layer near the membrane. It also affects the determined porosity (Fig. 6c), which decreases from 0.435 to 0.271 at the air inlet and to 0.141 at the air outlet. This significant reduction in porosity of 38% and 68% respectively increases the transport limitation for oxygen in the CCL and appears to contribute significantly to the performance decay.

The distribution of the catalyst layer components, which were already examined by the cross-sectional analysis, were further investigated by AFM measurements of the CCL surface (interface CCL/GDL). Fig. 7 shows high resolution AFM analysis of the CCL surface at BoT (a) as well as EoT at air inlet (b) and EoT at air outlet (c). In each case, an AFM topological image is shown along with a contact current distribution map as well as binarization of the contact current map into conductive and non-conductive areas using a threshold of 5 nA. Based on the height mapping, differences between BoT and EoT are not significant on the surface. For instance, only a slight change of surface porosity can be detected. From the surface porosity analysis, the BoT sample showed 22%, the air inlet sample 20% and the air outlet sample 17% surface porosity. However, when evaluating the electrical current mapping, the BoT sample (Fig. 7a) shows a conductive area of 54%, which becomes significantly reduced upon the degradation test. This results in conductive areas of 40% for the EoT sample near the air inlet (Figs. 7b) and 22% near the air outlet (Fig. 7c). The decrease of conductivity can be attributed to higher local ionomer concentration in the CCL because the ionomer is not conductive while the catalyst materials (Pt and carbon) are. Consequently, the ionomer concentration in the CCL increases relative to the Pt/C amount in the CCL during the 500 h test and the extent of the increase appears to depend on the operating conditions. The dry conditions near the air inlet (air feed with 30% RH) result in an ionomer concentration increase of about 26%. In contrast, the conditions at the air outlet are very humid due to the accumulation of product water along the air flow field. Here, the ionomer concentration increases by around 59%. This relative increase can have different causes. On the one hand, carbon corrosion and Pt loss (for example due to Pt dissolution and Pt band formation) can reduce the amount of catalyst material. On the other hand, a certain degree of ionomer mobility can result in a movement of ionomer chains within the CCL or from the membrane to the CCL.

It is well known, that the carbon corrosion rate increases with increasing relative humidity and with the presence of liquid water [52] [53]. Thus, a higher carbon corrosion rate can be expected close to the air outlet where the loss of the conductive area observed via AFM is particularly high. This aspect and the detected reduction of CCL thickness suggest that carbon corrosion could at least partially cause the compositional change in the CCL. However, the increase in ionomer concentration in the CCL by 26-59% is significantly higher than the decrease in CCL thickness by 11% would suggest. Thus, ionomer mobility also appears to contribute to this change, as existing pores in the CCL could be felt with migrating ionomer. Yin et al. [19] have shown that ionomer migration plays an important role in the structure changes of the CL and is influenced by changes of the humidity in the CL. The ionomer hydrates and dehydrates when the humidity in the CL increases and decreases. The resulting swelling and shrinking can induce ionomer migration due to irreversible viscoelastic strain [54]. It was found that a high amplitude of the humidity change promotes the ionomer migration and thus structural changes. The work of Yin et al. [19] was focused on the impact of this ionomer migration on the crack growth and propagation within the CL. Even without fuel cell operation, it was demonstrated that the electrochemical active surface area (ECSA) decreases and ORR charge transfer resistance increases due to hindered electron/ion pathways and detachment of catalyst/ionomer interfaces as a result of structural changes. Additionally, an increase of the O_2 mass transport resistance indicated a deterioration in mass transfer pathways in the CL due to ionomer migration and agglomeration in the CL pores.

In the experiments of the present work, the degradation test was realized by fuel cell operation in a technical cell, with low relative humidity at the air inlet and high relative humidity at the air outlet. Due to the different load levels in the FC-DLC and the included start-up and shut-down cycles, humidity is changing during the experiment. This enables the ionomer migration mechanism proposed by Yin et al. [19] and suggests that it is more pronounced at the air outlet. These aspects support the hypothesis that a significant part of the performance decrease in the 500 h test is caused not only by catalyst degradation but also by structural changes in the CCL due to ionomer migration. The corresponding ionomer mobility leads to an accumulation of the ionomer in the CCL, especially near the cathode/membrane interface and close to the air outlet. Consequently, the porosity is impeded there. However, it is not clear whether the additional ionomer in the CCL pores originates from the CCL or from the membrane. Additional ionomer from the membrane would lead to a reduced porosity and electronic

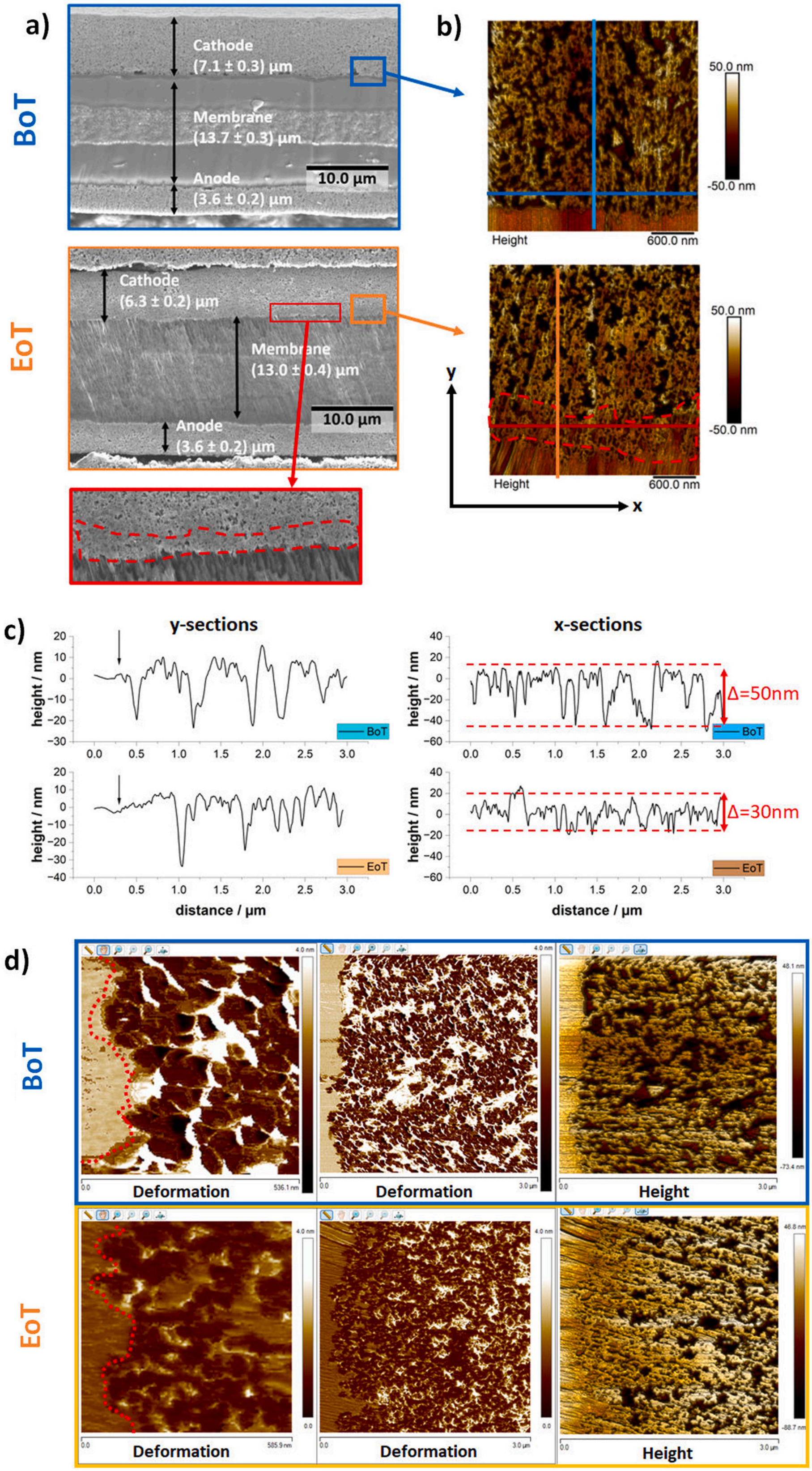

Fig. 5. BoT and EoT cathode (air inlet) catalyst layer structure evaluation based on cross-section analysis via (a) SEM and (b) AFM height analysis. The inset of the EoT SEM and the red dashed area in EoT SEM and AFM indicate the area with increased density. (c) Height profiles (line scans) are extracted from AFM by x- and y-sections as marked in (b). The vertical arrows in the y-section plots label the position of the membrane/CCL interface. (d) AFM deformation and height analysis of MEA cross-sections BoT and EoT. (For interpretation of the references to colour in this figure legend, the reader is referred to the Web version of this article.)

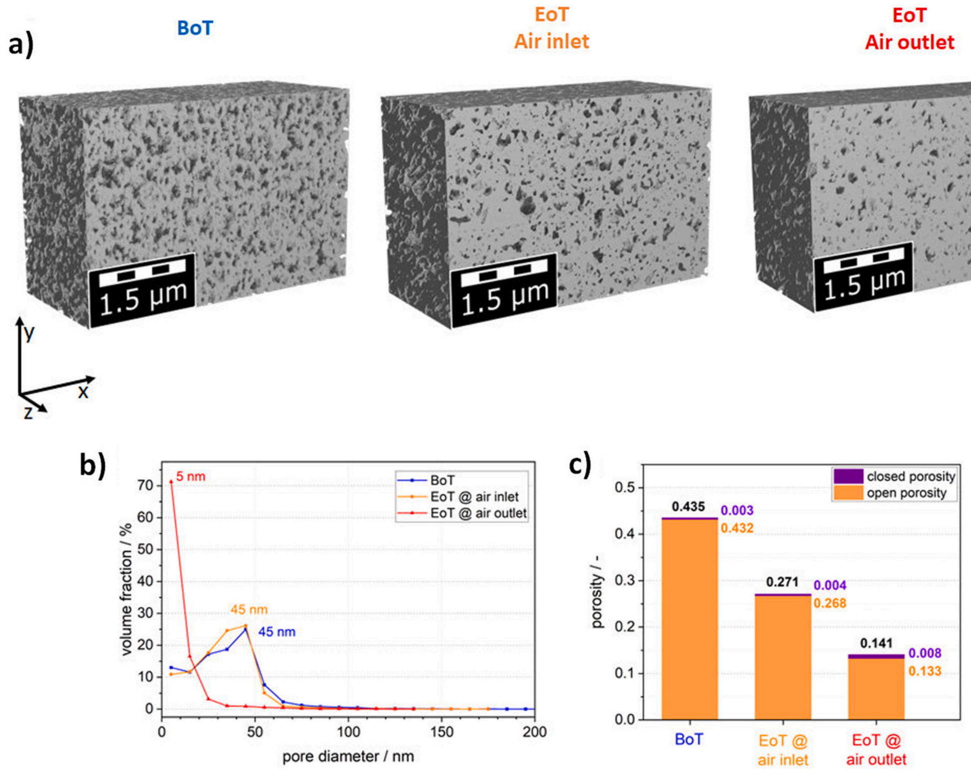

Fig. 6. FIB-SEM analysis of the CCL structures close to the membrane. (a) 3D reconstruction of CCL structure BoT and EoT at air inlet and air outlet. Y-direction represents gradient from membrane (bottom) towards GDL for a thickness of 3 µm. (b) Resulting pore size distribution in the examined CCLs. (c) Resulting porosity in the examined CCLs.

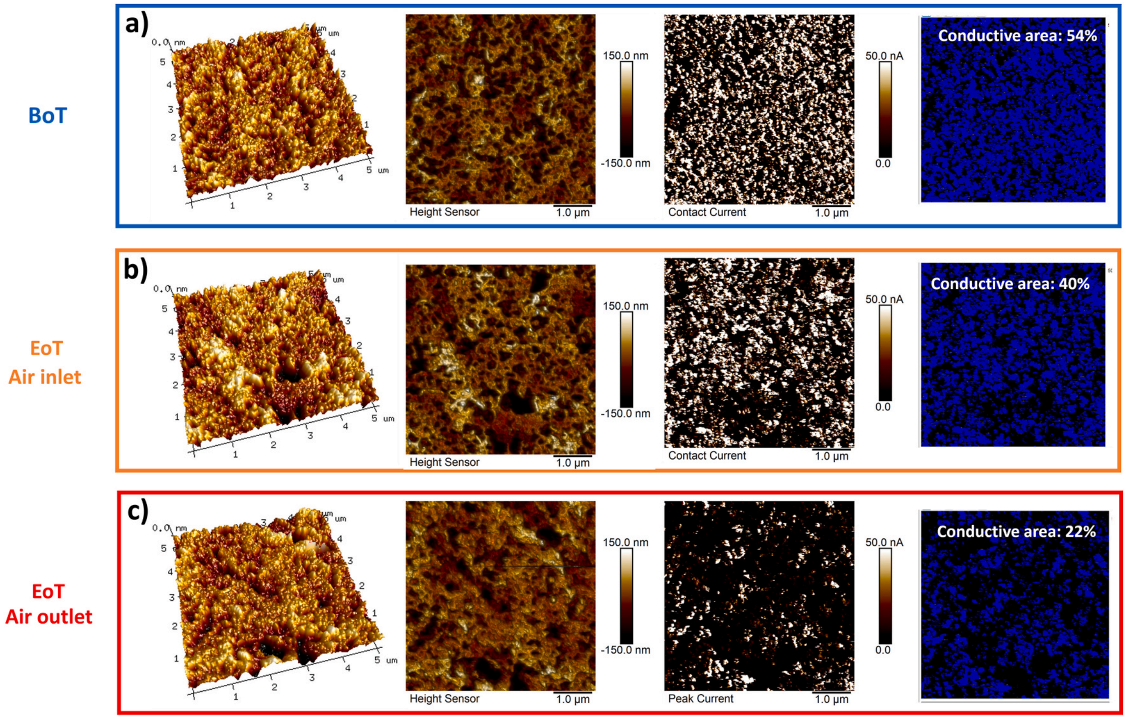

Fig. 7. Structural analysis of the cathode catalyst layer surface via AFM using height sensor (left), contact current (middle) and visualization of conductive area (right, blue: conductive, black: non-conductive using 5 nA threshold). Results are presented for (a) pristine BoT cathode as well as EoT samples located at (b) air inlet and (c) air outlet. (For interpretation of the references to colour in this figure legend, the reader is referred to the Web version of this article.)

conductivity at a large portion of the CCM, while a migration of the ionomer only in the catalyst layer would lead to ionomer depletion zones and zones with ionomer agglomeration. But neither of these two effects could be proven beyond doubt.

As shown in Fig. 8a via EIS at 1.5 A cm^{-2}, the O_2 mass transport resistance increases during the test from 107.0 to 117.8 mΩ cm^2 by about 10% (also see Fig. S1 and Table S2), which might be caused by the decreased porosity in the CCL and by the increase of the ionomer film thickness on the Pt/C catalyst.

3.5. Impact on proton conductivity

The increase of the local ionomer concentration in the CCL affects additionally the proton conductivity of this layer. This aspect is analyzed by EIS measurements in hydrogen/nitrogen at variable relative humidity as shown in Fig. 8b. The resulting effective proton transport resistances are shown in Fig. 8c and it is obvious that these values decrease significantly during the 500 h test. The more humid the measuring conditions are, the more this resistance decreases, by about 25% at 50% RH, over 34% at 80% RH, up to 38% at 100% RH. This very significant decrease in the effective proton transport resistance demonstrates that the ionomer network in the CCL has become much denser, which facilitates proton transport but hinders oxygen transport.

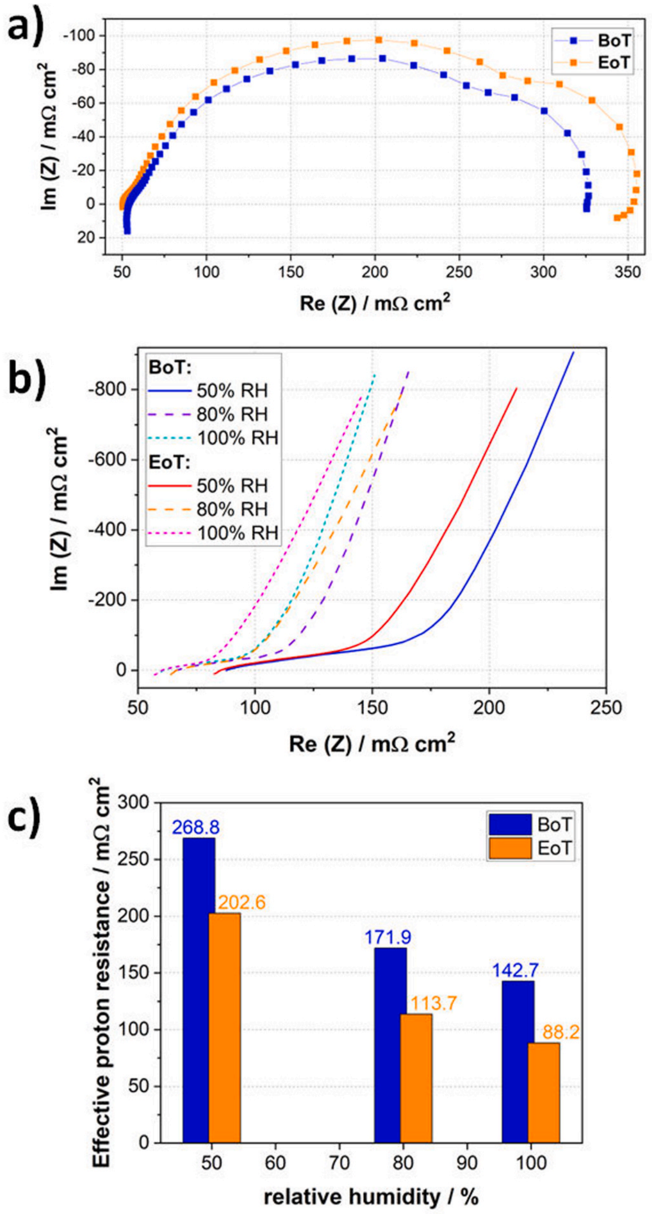

Fig. 8. Impact of 500 h degradation test on transport properties in the CL by BoT and EoT analysis via: (a) Nyquist plots of EIS at 1.5 A cm^{-2} in hydrogen/air using automotive test conditions (80 °C, 2.5/2.3 bar$_{abs}$, 50%/30% RH and 1.3/1.5 stoichiometry at anode and cathode, respectively); Bode plots presented in Fig. S5, (b) Nyquist plots of EIS at 0.4 V in hydrogen/nitrogen at 80 °C and 1500 mbar$_{abs}$ using variable relative humidity; Bode plots presented in Fig. S6 as well as (c) resulting effective proton transport resistances.

It should also be mentioned that the work of Yin et al. [19] has shown that the proton transport resistance can also increase when cracks form and propagate in the CCL, interrupting the proton transport pathways. However, since CCLs used in the present work did not show any cracks (see Fig. 3), this effect does not occur here.

4. Conclusion

This work presents a detailed study regarding the impact of a 500 h FC-DLC degradation test on transport and structural properties in the CCL. A 22.5 cm^2 technical single cell with significant differences in the operating conditions at air inlet and air outlet is used to evaluate local effects. The examined CCM uses a commercial Pt/C catalyst and a cathode platinum loading of 0.2 mg cm^{-2}.

This test resulted in significant performance degradation of up to 110 mV at 2.0 A cm^{-2}. The detailed analysis of the degradation processes firstly focused on the used materials. Membrane degradation was not the main focus of the presented work and demonstrated a minor effect on the performance loss.

As known from the literature [55], the low current density regime in polarization curves is dominated by the ORR charge transfer resistance. The performance decay analyzed in this regime at 0.05 A cm^{-2} showed a degradation rate of −42 μV h^{-1}. This can be attributed to irreversible catalyst degradation as indicated by the ECSA loss of 37% and Pt redeposition in the membrane as platinum band. These changes resulted in 24% increase in the ORR charge-transfer resistance. In general, oxygen transport limitation becomes more important with increasing current density [55]. The analyzed voltage decay in this regime is more pronounced with increasing current density and the degradation rates of −98 μV h^{-1} at 0.44 A cm^{-2} as well as −122 μV h^{-1} at 1.05 A cm^{-2} cannot only be attributed to material changes, but also to increased oxygen transport limitations. Thereby, the oxygen transport is primarily affected by the CL structure. A closer look on the pore structure in the CCL reveals that an about 0.6 μm thick layer with drastically reduced porosity by 40% has formed at the CCL/membrane interface.

The combination of FIB-SEM and AFM deformation and height analysis confirms the formation of this dense layer and the loss of porosity at the CCL/membrane interface by 38% and 68% at air inlet and air outlet, respectively. Supplementary to the potential collapse of the pore structure due to carbon corrosion and catalyst degradation, ionomer migration was identified by these AFM measurements to cause the changes at the CCL/membrane interface by filling the pores with ionomer. Thereby, pore diameter and the pore volume are significantly reduced. In addition to the effect at the CL/membrane interface, an increase of the local ionomer concentration relative to the Pt/C amount was observed at the surface of the CL which, in contrast to the dense layer at CL/membrane interface, does not lead to topography changes. It is well known that changes in humidity results in swelling and shrinking of the ionomer and this can induce ionomer migration in the CL. Due to the more humid local conditions at air outlet, the ionomer seems to be more mobile there. On cell level, this increased ionomer concentration in the catalyst layers results in a reduction of the effective proton transport resistance by up to 38% and an increase of the O_2 transport resistance by about +10%.

The presented work reveals that the ionomer migrates in the CCL during application relevant fuel cell operation on a macroscopic level. The impact of ionomer mobility on property changes of nanoscale thin-films and catalyst/ionomer interactions or CL morphological changes is well known. But this effect is strongly influenced by local operating conditions and thus required in-situ examination regarding CCL properties changes including the porosity. Thereby, it is shown that the local humidity level in the CCL is of high importance to evaluate the impact of this important performance degradation mechanism during fuel cell operation.

CRediT authorship contribution statement

J. Mitzel: Conceptualization, Investigation, Methodology, Writing – original draft. **T. Morawietz:** Investigation, Visualization, Writing – review & editing. **J.-F. Heger:** Software, Visualization, Writing – review & editing. **H. Kaess:** Funding acquisition, Validation, Writing – review & editing. **P. Gazdzicki:** Funding acquisition, Supervision, Validation, Writing – review & editing.

Declaration of competing interest

The authors declare that they have no known competing financial interests or personal relationships that could have appeared to influence the work reported in this paper.

Acknowledgements

The research leading to these results has received funding from the Fuel Cells and Hydrogen 2 Joint Undertaking (now Clean Hydrogen Partnership) under Grant Agreement No 875025 (Further-FC). This Joint Undertaking receives support from the European Union's Horizon 2020 Research and Innovation program, Hydrogen Europe and Hydrogen Europe Research.

The authors gratefully acknowledge Siegfried Graf and Stefan Anderle for the installation of the used test equipment and the development of the LabView applications for test bench control as well as data acquisition and visualization.

Appendix A. Supplementary data

Supplementary data to this article can be found online at https://doi.org/10.1016/j.jpowsour.2026.240392.

Acronyms

AFM	Atomic Force Microscopy
AST	Accelerated stress test
BoT	Begin-of-test
CCL	cathode catalyst layer
CCM	catalyst coated membrane
CL	catalyst layer
CV	cyclic voltammetry
ECSA	electrochemical active surface area
EIS	electrochemical impedance spectroscopy
EoT	End-of-test
FC-DLC	Fuel Cell Dynamic Load Cycle
GDL	Gas diffusion layer
ICE	internal combustion engines
MEA	Membrane electrode assembly
O_2	Oxygen
ORR	oxygen reduction reaction
PEMFC	Polymer electrolyte membrane fuel cells
Pt	Platinum
Pt/C	Platinum on carbon catalyst
PTFE	Polytetrafluoroethylene
SEM	Scanning Electron Microscopy
TPB	triple phase boundary

Symbols

A_{geo}	geometric active area of the examined electrode/22.5 cm^2
C_{dl}	double layer capacity/mF cm_{geo}^{-2}
HFR	high frequency resistance/mOhm cm^2
I_{dl}	current in double layer region at 0.45 V corrected by hydrogen crossover current/A
$q_{H\text{-}ads}$	charge of the hydrogen adsorption peaks in CV/C
$R_{eff,H+}$	effective proton transport resistance/mOhm cm^2
RF	roughness factor/cm_{Pt}^2 cm_{geo}^{-2}
RH	relative humidity/%
v	voltage scan rate of the CV measurement/mV s^{-1}
x_{war}	magnitude of a Warburg-like region projected onto the x-axis in a Nyquist plot/mOhm cm^2
Γ	charge for the electrochemical adsorption of one monolayer hydrogen on a polycrystalline platinum surface/210 µC cm_{Pt}^{-2}

Data availability

Data will be made available on request.

References

[1] A.N. Mancino, C. Menale, F. Vellucci, M. Pasquali, R. Bubbico, PEM fuel cell applications in road transport, Energies 16 (2023) 6129, https://doi.org/10.3390/en16176129.

[2] D. Hart, S. Jones, X. Cordobes, G. Bates, J. Lewis. The fuel cell industry review 2022. The ERM International Group Limited. https://www.erm.com/contentassets/55c43361e857413387f28fbacea6e91a/the-fuel-cell-industry-review-2022.pdf.

[3] A. Alaswad, A. Omran, J.R. Sodre, T. Wilberforce, G. Pignatelli, M. Dassisti, A. Baroutaji, A.G. Olabi, Technical and commercial challenges of proton-exchange membrane (PEM) fuel cells, Energies 14 (2021) 144, https://doi.org/10.3390/en14010144.

[4] S.T. Thompson, D. Papageorgopoulos, Nat. Catal. 2 (2019) 558–561. https://www.nature.com/articles/s41929-019-0291-x.

[5] N. Zamel, The catalyst layer and its dimensionality – a look into its ingredients and how to characterize their effects, J. Power Sources 309 (2016) 141–159, https://doi.org/10.1016/j.jpowsour.2016.01.091.

[6] Clean hydrogen joint undertaking; SRIA key performance indicators (KPIs). https://www.clean-hydrogen.europa.eu/knowledge-management/strategy-map-and-key-performance-indicators/clean-hydrogen-ju-sria-key-performance-indicators-kpis_en, 2022.

[7] P. Ren, P. Pei, Y. Li, Z. Wu, D. Chen, S. Huang, Degradation mechanisms of proton exchange membrane fuel cell under typical automotive operating conditions, Prog. Energy Combust. Sci. 80 (2020) 100859, https://doi.org/10.1016/j.pecs.2020.100859.

[8] J. Mitzel, Q. Zhang, P. Gazdzicki, K.A. Friedrich, Review on mechanisms and recovery procedures for reversible performance losses in polymer electrolyte membrane fuel cells, J. Power Sources 488 (2021) 229375, https://doi.org/10.1016/j.jpowsour.2020.229375.

[9] Q. Zhang, C. Harms, J. Mitzel, P. Gazdzicki, K.A. Friedrich, The challenges in reliable determination of degradation rates and lifetime in polymer electrolyte membrane fuel cells, Curr. Opin. Electrochem. 31 (2022) 100863, https://doi.org/10.1016/j.coelec.2021.100863.

[10] J. Zhao, H. Liu, X. Li, Structure, property, and performance of catalyst layers in proton exchange membrane fuel cells, Electrochem. Energy Rev. 6 (2023) 13, https://doi.org/10.1007/s41918-022-00175-1.

[11] M. Yue, X. Si, J. Zhang, et al., A comprehensive review of PEMFC durability in dynamic operation: critical stressors, degradation analysis, and lifetime prognostics, Energy Convers. Manag. 30 (2026) 101866, https://doi.org/10.1016/j.ecmx.2026.101866.

[12] S. Zhang, X.-Z. Yuan, et al., A review of platinum-based catalyst layer degradation in proton exchange membrane fuel cells, J. Power Sources 194 (2009) 588–600, https://doi.org/10.1016/j.jpowsour.2009.06.073.

[13] P. Novotny, M. Tomas, T. Nemec, et al., On/off cycling test of low-temperature PEM fuel cell at fully humidified conditions, Int. J. Green Energy 16 (2019) 1189–1195, https://doi.org/10.1080/15435075.2019.1671394.

[14] J. Zhao, S. Shahgaldi, X.G. Li, et al., Experimental observations of microstructure changes in the catalyst layers of proton exchange membrane fuel cells under wet-dry cycles, J. Electrochem. Soc. 165 (2018) F3337–F3345, https://doi.org/10.1149/2.0391806jes.

[15] Y. Singh, R.T. White, M. Najm, et al., Tracking the evolution of mechanical degradation in fuel cell membranes using 4D in situ visualization, J. Power Sources 412 (2019) 224–237, https://doi.org/10.1016/j.jpowsour.2018.11.049.

[16] E. Guilminot, A. Corcella, M. Chatenet, et al., Membrane and active layer degradation upon PEMFC steady-state operation, J. Electrochem. Soc. 154 (2007) B1106–B1114, https://doi.org/10.1149/1.2775218.

[17] S. Helmly, R. Hiesgen, T. Morawietz, et al., Microscopic investigation of platinum deposition in PEMFC cross-sections using AFM and SEM, J. Electrochem. Soc. 160 (2013) F687, https://doi.org/10.1149/2.130306jes.

[18] R.L. Borup, A. Kusoglu, K.C. Neyerlin, R. Mukundan, R.K. Ahluwalia, D.A. Cullen, K.L. More, A.Z. Weber, D.J. Myers; Recent developments in catalyst-related PEM fuel cell durability; Curr. Opin. Electrochem. 21 (2020) 192-200; https://doi.org/10.1016/j.coelec.2020.02.007.

[19] Z. Fang, A.G. Star, T.F. Fuller, Effect of carbon corrosion on wettability of PEM fuel cell electrodes, J. Electrochem. Soc. 166 (2019) F709, https://doi.org/10.1149/2.0231912jes. https://iopscience.iop.org/article/10.1149/2.0231912jes/meta.

[20] D. Garcia-Sanchez, T. Morawietz, P. Gama da Rocha, R. Hiesgen, P. Gazdzicki, K. A. Friedrich, Local impact of load cycling on degradation in polymer electrolyte fuel cells, Appl. Energy 259 (2020) 114210, https://doi.org/10.1016/j.apenergy.2019.114210.

[21] R. Sharma, P. Morgen, S. Chiriaev, P. Brilner Lund, M. Juul Larsen, B. Sieborg, L. Grahl-Madsen, S.M. Andersen, Insights into degradation of the membrane–electrode assembly performance in low-temperature PEMFC: the catalyst, the ionomer, or the interface? CS Applied Materials & Interfaces 44 (2022) 49658–49671, https://doi.org/10.1021/acsami.2c12327. https://pubs.acs.org/doi/full/10.1021/acsami.2c12327.

[22] T. Morawietz, M. Handl, C. Oldani, K.A. Friedrich, R. Hiesgen, Quantitative in situ analysis of ionomer structure in fuel cell catalytic layers, ACS Appl. Mater. Interfaces 8 (2016) 27044–27054. https://pubs.acs.org/doi/10.1021/acsami.6b07188.

[23] T. Morawietz, M. Handl, C. Oldani, P. Gazdzicki, J. Hunger, F. Wilhelm, J. Blake, K. A. Friedrich, R. Hiesgen, High-resolution analysis of ionomer loss in catalytic layers after operation, J. Electrochem. Soc. 165 (2018), https://doi.org/10.1149/2.0151806jes.

[24] A.P. Soleymani, M. Reid, J. Jankovic, An epoxy-free sample preparation approach to enable imaging of ionomer and carbon in polymer electrolyte membrane fuel cells, Adv. Funct. Mater. 33 (2023) 2209733, https://doi.org/10.1002/adfm.202209733.

[25] L. Hu, T.V. Cleve, H.n Yu, J.H. Park, N. Kariuki, A.J. Kropf, R. Mukundan, D. A. Cullen, D.J. Myers, K.C. Neyerlin, Electrochemical characterization of evolving ionomer/electrocatalyst interactions throughout accelerated stress tests, J. Power Sources 556 (2023) 232490, https://doi.org/10.1016/j.jpowsour.2022.232490.

[26] F. Chabot, P. Lionel, L. Guétaz, S. Rosini, A. Morin, Tracking the evolution of ionomer film and catalyst material to unravel PEMFC performance degradation, J. Electrochem. Soc. 171 (2024) 124506, https://doi.org/10.1149/1945-7111/ada111.

[27] W. He, F. Tang, X. Li, et al., Quantification and evolution on degradation mechanisms of proton exchange membrane fuel cell catalyst layer under dynamic testing conditions, Int. J. Hydrogen Energy 48 (2023) 18032, https://doi.org/10.1016/j.ijhydene.2023.01.109.

[28] J. Wang, J. Geng, M. Wang, Quantification on degradation mechanisms of polymer exchange membrane fuel cell cathode catalyst layers during bus and stationary durability test protocols, J. Power Sources 521 (2022) 230878, https://doi.org/10.1016/j.jpowsour.2021.230878.

[29] Y. Xiao, W. Zheng, J. Wang, et al., Degradation behavior of ionomer in the cathode catalyst layer of polymer electrolyte fuel cells, Appl. Energy 389 (2025) 125759, https://doi.org/10.1016/j.apenergy.2025.125759.

[30] Y. Yin, R. Li, F. Bai, W. Zhu, Y. Qin, Y. Chang, J. Zhang, M.D. Guiver, Ionomer migration within PEMFC catalyst layers induced by humidity changes, Electrochem. Commun. 109 (2019) 106590, https://doi.org/10.1016/j.elecom.2019.106590.

[31] G. Tsotridis, A. Pilenga, G. De Marco, T. Malkow, EU harmonised test protocols for PEMFC MEA testing in single cell configuration for automotive applications, JRC Sci. Policy Rep (2015), https://doi.org/10.2790/54653.

[32] P. Gazdzicki, J. Mitzel, D. Garcia Sanchez, M. Schulze, K.A. Friedrich, Evaluation of reversible and irreversible degradation rates of polymer electrolyte membrane fuel cells tested in automotive conditions, J. Power Sources 327 (2016) 86–95, https://doi.org/10.1016/j.jpowsour.2016.07.049.

[33] Y. Ishigami, K. Takada, H. Yano, J. Inukai, M. Uchida, Y. Nagumo, T. Hyakutake, H. Nishide, M. Watanabe, Corrosion of carbon supports at cathode during hydrogen/air replacement at anode studied by visualization of oxygen partial pressures in a PEFC—Start-up/shut-down simulation, J. Power Sources 196 (2011) 3003–3008, https://doi.org/10.1016/j.jpowsour.2010.11.092.

[34] M.C. Lefebvre, R.B. Martin, P.G. Pickup, Characterization of ionic conductivity profiles within proton exchange membrane fuel cell gas diffusion electrodes by impedance spectroscopy, Electrochem. Solid State Lett. 2 (1999) 259, https://doi.org/10.1149/1.1390804. https://iopscience.iop.org/article/10.1149/1.1390804.

[35] G. Li, P.G. Pickup, Ionic conductivity of PEMFC electrodes: effect of nafion loading, J. Electrochem. Soc. 150 (2003) C745, https://doi.org/10.1149/1.1611493. https://iopscience.iop.org/article/10.1149/1.1611493.

[36] K. Kinoshita, P. Stonehart, Chapter "Preparation and Characterization of Highly Dispersed Electrocatalytic Materials", in: Modern Aspects of Electrochemistry, Springer, Boston, MA, 1977 https://doi.org/10.1007/978-1-4615-7452-1_4.

[37] F. Gloaguen, J.-M. Léger, C. Lamy, Electrocatalytic oxidation of methanol on platinum nanoparticles electrodeposited onto porous carbon substrates, J. Appl. Electrochem. 27 (1997) 1052–1060, https://doi.org/10.1023/A:1018434609543.

[38] Y. Qi, et al., Insight into carbon corrosion of different carbon supports for Pt-based electrocatalysts using accelerated stress tests in polymer electrolyte fuel cells, J. Power Sources 551 (2022) 232209, https://doi.org/10.1016/j.jpowsour.2022.232209.

[39] A.P. Young, J. Stumper, E. Gyenge, Characterizing the structural degradation in a PEMFC cathode catalyst layer: carbon corrosion, J. Electrochem. Soc. 156 (2009) B913, https://doi.org/10.1149/1.3139963. https://iopscience.iop.org/article/10.1149/1.3139963/meta.

[40] M.V. Williams, H. Russell Kunz, J.M. Fenton, Analysis of polarization curves to evaluate polarization sources in hydrogen/air PEM fuel cells, J. Electrochem. Soc. 152 (2005) A635, https://doi.org/10.1149/1.1860034.

[41] D. Garcia-Sanchez, T. Morawietz, P. Gama da Rocha, R. Hiesgen, P. Gazdzicki, K. A. Friedrich, Local impact of load cycling on degradation in polymer electrolyte fuel cells, Appl. Energy 259 (2020) 114210, https://doi.org/10.1016/j.apenergy.2019.114210.

[42] T. Jahnke, G.A. Futter, A. Baricci, C. Rabissi, A. Casalegno, Physical modeling of catalyst degradation in low temperature fuel cells: platinum oxidation, dissolution, particle growth and platinum band formation, J. Electrochem. Soc. 167 (2019) 013523, https://doi.org/10.1149/2.0232001JES. https://iopscience.iop.org/article/10.1149/2.0232001JES/meta.

[43] H. Liu, J. Zhang, F.D. Coms, W. Gu, B. Litteer, H.A. Gasteiger, Impact of gas partial pressure on PEMFC chemical degradation, ECS Trans. 3 (2006) 493, https://doi.org/10.1149/1.2356171.

[44] Z. Luo, Z. Chang, Y. Zhang, Z. Liu, J. Li, Electro-osmotic drag coefficient and proton conductivity in nafion membrane for PEMFC, Int. J. Hydrogen Energy 35 (2010) 3120, https://doi.org/10.1016/j.ijhydene.2009.09.013.

[45] T.S. Kassa, A.M. Yessuf, M.M. Mohideen, A.M. Mihiretu, S. Ramakrishna, Y. Liu, Modification, degradation, and mitigation of perfluorosulfonic acid proton exchange membranes for fuel cells: a review, ACS Appl. Mater. Interfaces 17 (2025) 45271, https://doi.org/10.1021/acsami.5c02335.

[46] T. Ma, G. Jing, C. Hu, Y. Qin, X. Sun, Research on the mechanisms of contact resistance and structural deformation impact on PEMFC performance, Case Stud. Therm. Eng. 74 (2025) 106845, https://doi.org/10.1016/j.csite.2025.106845.

[47] S. Prass, J. St-Pierre, M. Klingele, K.A. Friedrich, N. Zamel, Hydrogen oxidation artifact during platinum oxide reduction in cyclic voltammetry analysis of low-loaded PEMFC electrodes, Electrocatalysis 12 (2021) 45–55, https://doi.org/10.1007/s12678-020-00627-6.

[48] S. Jomori, N. Nonoyama, T. Yoshida, Analysis and modeling of PEMFC degradation: effect on oxygen transport, J. Power Sources 215 (2012) 18, https://doi.org/10.1016/j.jpowsour.2012.04.069.

[49] H. Iden, A. Ohma, An in situ technique for analyzing ionomer coverage in catalyst layers, J. Electroanal. Chem. 693 (2013) 34–41, https://doi.org/10.1016/j.jelechem.2013.01.026.

[50] L. Dubau, L. Castanheira, F. Maillard, M. Chatenet, O. Lottin, G. Maranzana, J. Dillet, A. Lamibrac, J.C. Perrin, E. Moukheiber, A. ElKaddouri, G. De Moor, C. Bas, L. Flandin, N. Caqué, A review of PEM fuel cell durability: materials degradation, local heterogeneities of aging and possible mitigation strategies, WIREs Energy Environ. 3 (2014) 540–560, https://doi.org/10.1002/wene.113.

[51] T. Soboleva, K. Malek, Z. Xie, T. Navessin, S. Holdcroft, PEMFC catalyst layers: the role of micropores and mesopores on water sorption and fuel cell activity, ACS Appl. Mater. Interfaces 3 (2011) 1827–1837, https://doi.org/10.1021/am200590w.

[52] K.H. Lim, H.-S. Oh, S.-E. Jang, Y.-J. Ko, H.-J. Kim, H. Kim, Effect of operating conditions on carbon corrosion in polymer electrolyte membrane fuel cells, J. Power Sources 193 (2009) 575–579, https://doi.org/10.1016/j.jpowsour.2009.04.006.

[53] T. Mittermeier, A. Weiß, F. Hasché, H.A. Gasteiger, PEM fuel cell start-up/shut-down losses vs relative humidity: the impact of water in the electrode layer on carbon corrosion, J. Electrochem. Soc. 165 (2018) F1349, https://doi.org/10.1149/2.0931816jes. https://iopscience.iop.org/article/10.1149/2.0931816jes/meta.

[54] D.L. Wood, J. Chlistunoff, J. Majewski, R.L. Borup, Nafion structural phenomena at platinum and carbon interfaces, J. Am. Chem. Soc. 131 (2009) 18096–18104, https://doi.org/10.1021/ja9033928. https://pubs.acs.org/doi/10.1021/ja9033928.

[55] M. Arif, S.C.P. Cheung, J. Andrews, A systematic approach for matching simulated and experimental polarization curves for a PEM fuel cell, Int. J. Hydrogen Energy 45 (2020) 2206, https://doi.org/10.1016/j.ijhydene.2019.11.057.